# Görtler instability

S. A. Ragab and A. H. Nayfeh

Citation: Physics of Fluids (1958-1988) **24**, 1405 (1981); doi: 10.1063/1.863557
View online: http://dx.doi.org/10.1063/1.863557
View Table of Contents: http://scitation.aip.org/content/aip/journal/pof1/24/8?ver=pdfcov
Published by the AIP Publishing



# Görtler instability

S. A. Ragab and A. H. Nayfeh[a)]

*Department of Engineering Science and Mechanics, Virginia Polytechnic Institute and State University, Blacksburg, Virginia 24061*

(Received 28 December 1979; accepted 20 May 1981)

Görtler instability for boundary-layer flows over generally curved walls is considered. The full-linearized disturbance equations are obtained in an orthogonal curvilinear coordinate system. A perturbation procedure to account for second-order effects is used to determine the effects of the displacement thickness and the variation of the streamline curvature on the neutral stability of the Blasius flow. The streamwise pressure gradient in the mean flow is accounted for by solving the nonsimilar boundary-layer equations. Growth rates are obtained for the actual mean flow and compared with those for the Blasius flow and the Falkner–Skan flows. The results demonstrate the strong influence of the streamwise pressure gradient and the nonsimilarity of the basic flow on the stability characteristics.

## I. INTRODUCTION

Centrifugal instability in boundary-layer flows over concavely curved walls was first demonstrated theoretically by Görtler.[1] The disturbances are in the form of counter-rotating streamwise vortices, called Görtler vortices. Indirect evidence of the instability of the flow over a concave wall was provided by Clauser and Clauser[2] who observed that a laminar boundary-layer flow over a concave wall became turbulent at Reynolds numbers that are smaller than those for boundary-layer flows over flat or convex walls. Liepmann[3,4] found that the Görtler number correlates the stability conditions. Using the china-clay technique, Gregory and Walker[5] were the first to observe traces of Görtler vortices. Then, Aihara[6] and Tani and Sakagami[7] used colored liquids and smoke threads to visualize these vortices. Subsequently, Wortmann[8,9] used the tellurium method to visualize these vortices in a water tunnel. Bippes[10] and Bippes and Görtler[11] presented the most detailed visualization of these vortices using the hydrogen-bubble technique. Their experiments were conducted on walls with the radii 0.5 and 1.0 m so that the generated vortices were fairly strong. Using hot-wire measurements, Aihara[6] and Tani[12,13] found three-dimensional counter-rotating vortices with spanwise vorticity in a boundary layer over a concave wall.

These vortices by themselves may not lead to the transition of laminar flows to turbulent flows. The influence of steady streamwise vortices on two-dimensional Tollmien–Schlichting waves was studied experimentally by Tani,[12] Aihara,[6] Tani and Sakagami,[7] Tani and Aihara,[14] Bippes,[10] and Wortmann.[15] Aihara,[6] and Tani and Aihara[14] concluded that the Görtler vortices indirectly affect the transition by inducing a spanwise variation in the boundary-layer thickness, at least when the radii of curvature are not extremely small. Tani[12] found the spatial amplification of the Görtler vortices to be small, even at downstream locations close to the transition point. However, these vortices deform the mean flow field and induce a spanwise variation in the boundary-layer thickness, resulting in the development of velocity profiles having varying stability characteristics along the span. The modification of the mean flow modifies the amplification of the unsteady waves. Wortmann[15] observed a secondary steady instability following the appearance of the Görtler vortices before three-dimensional unstable waves that lead to transition set in. Bippes[10] and Aihara[16] observed meandering or pulsating vortices before turbulence sets in. Thus, available experimental evidence indicates that the Görtler vortices do not lead directly to turbulence without a coupling with unsteady two- or three-dimensional unstable disturbances. Motivated by the experimental evidence, Nayfeh[17] presented a theoretical model for studying the effect of streamwise vortices on Tollmien–Schlichting waves. He showed that such vortices have a strong tendency to amplify three-dimensional Tollmien–Schlichting waves having a spanwise wavelength that is twice the wavelength of the vortices. Therefore, the study of Görtler instability is of importance not only in heat exchange problems but also in the analysis of the transition region over concavely curved walls.

In his analysis, Görtler assumed the boundary layer to be parallel, the pressure gradients to be negligible, the curvature of the streamlines to be the same constant at all distances normal to the wall and equal to the curvature of the wall, and the vortices to be confined to the boundary layer. He used Green's functions to transform the resulting eigenvalue problem into an integral equation, which he then solved. Hämmerlin[18] resolved Görtler's simplified equations and found that the vortices reach far beyond the edge of the boundary layer at small spanwise wavenumbers. Consequently, he[19] dropped Görtler's assumption that the vortices are confined to the boundary layer and modified Görtler's equations.

Using a body-oriented coordinate system, Smith[20] rederived the eigenvalue problem, including the effects of the variation of the streamline curvature and the normal velocity component. The resulting equations contain the factors $(1-ky)^{-n}$, where $n$ is an integer, $k$ is the curvature of the wall, and $y$ is the distance normal to the wall. To remove the singularity from the finite location $y=k^{-1}$, Smith replaced these factors by the first two terms $1+nky$ in their Taylor series expansions. Alternatively, Schultz-Grunow and Behbahani[21] did not approximate the factors $(1-ky)^{-n}$ and solved the eigenvalue problem subject to the condition that the perturbations vanish relative to the mean flow rather than

[a)]Present address: Tarmouk University, Irbid, Jordan.

 0031-9171/81/081405-13$00.90  

absolutely with increasing distance from the wall. However, one of their equations has an error, which was later corrected by Behbahani.[22] Alternatively, Hämmerlin[23] accounted for the variation of the streamline curvature normal to the wall by using a flow that has the properties of boundary-layer flows along a wavy wall in the valley positions. There, the streamline curvature decays like $\exp(-c\bar{\psi})$, where $\bar{\psi}$ represents the normal distance to the wall. He utilized the streamlines to construct a locally orthogonal curvilinear coordinate system. Tobak[24] considered the case of a wall having a finite extent of streamwise curvature. The effect of this curvature in the final equations appears as a multiplier to the Görtler number. Herbert[25] gave a comprehensive survey of the efforts of these authors and obtained very accurate numerical solutions to their models.

As mentioned earlier, Smith[20] incorporated the transverse component of the basic flow and some of the higher-order curvature terms. Furthermore, he considered spatially rather than temporally growing vortices. Smith's viewpoint is consistent with the experimental observations. Smith used body-oriented axes and a Taylor-series expansion of the metric coefficient for small distances normal to the wall. He kept two terms in the expansion. Kahawita and Meroney[26,27] used Smith's model and studied the influence of heating on the stability of laminar boundary layers along concave curved walls. They found that the inclusion of the normal velocity component changes the neutral curve drastically. Floryan and Saric[28] reformulated the problem in an orthogonal curvilinear coordinate system constructed from the potential lines and streamlines of the inviscid flow over the curved wall. They considered the case of a circular arc and obtained the basic approximations of the mean-flow and disturbance equations. Except for the streamwise variation of the transverse component of velocity, the stability equations of Floryan and Saric are the same as those of Smith if $(1-ky)^{-n}$ is approximated by 1 instead of $1+nky$.

Here, we are interested in the flow over walls with general distributions of curvature, in contrast with existing analyses, which treat circular arcs or circles. Specifically, we consider the effect of the streamwise pressure gradient on the stability characteristics. We employ a coordinate system based on the potential lines and streamlines. The inviscid flow and the metric coefficients of the coordinate system are obtained using the method of Davis[29] for constructing body-fitted coordinate systems. His method is based on the Schwarz–Christoffel transformation generalized for curved surfaces. In Sec. II, the two-dimensional basic-flow equations are derived in potential-line and streamline coordinates. In Sec. III, the complete linearized Navier–Stokes equations are derived for the disturbance quantities. The quasi-parallel-flow assumption and the normal-mode solution are discussed. Then, a method of solution is presented. Terms of order smaller than $O(1)$ are treated as perturbation quantities to a basic system that includes the $O(1)$ terms. The method of solution of the basic system is presented in Sec. IV. A new method of applying the asymptotic boundary condition far from the wall is presented. In Sec. V, a perturbation procedure is presented to account for small quantities in the disturbance equations. Results and their discussion are presented in Sec. VI.

## II. THE BASIC FLOW

We consider steady two-dimensional viscous incompressible flows over a curved wall. The fluid properties $\rho^*$ and $\mu^*$ are assumed to be constants. We employ an orthogonal curvilinear coordinate system $\phi^*$, $\psi^*$, and $z^*$, where $\phi^*$ and $\psi^*$ are the potential and stream functions of the two-dimensional inviscid flow over the given wall, respectively, and $z^*$ is a rectilinear coordinate normal to the plane of the basic motion. We choose $\psi^*=0$ to coincide with the body surface and $\phi^*=0$ to coincide with the leading edge. In this case, the metric coefficients $h^*_{\phi^*}$ and $h^*_{\psi^*}$ are equal to $U^{*-1}$, where $U^*(\phi^*,\psi^*)$ is the total inviscid velocity. Actually, it is the $\phi$ component of the inviscid velocity since the velocity normal to an inviscid streamline is by definition equal to zero. We introduce the following nondimensional variables:

$$\phi=\phi^*/U^*_\infty L^*, \quad \psi=\psi^*/U^*_\infty L^*, \tag{1}$$

$$h_\phi=h_\psi=h=U_\infty/U^*(\phi^*,\psi^*), \tag{2}$$

$$u=u^*/U^*_\infty, \quad v=v^*/U^*_\infty, \quad w=w^*/U^*_\infty, \quad p=p^*/\rho^*U^{*2}_\infty. \tag{3}$$

We define a characteristic Reynolds number $\mathrm{Re}=\rho^*U^*_\infty L^*/\mu^*$, where $U^*_\infty$, $\rho^*$, and $\mu^*$ are the free-stream values of velocity, density, and viscosity and $L^*$ is a characteristic length, the distance from the leading edge of the curved wall to the position of maximum height, see Fig. 1. We introduce the new variables

$$\tilde{u}=hu, \quad \tilde{v}=hv. \tag{4}$$

In terms of these variables, the first-order boundary-layer equations are given by[30]

$$\tilde{u}\frac{\partial\tilde{u}}{\partial\phi}+\tilde{v}\frac{\partial\tilde{u}}{\partial\psi}=\frac{1}{h}\frac{\partial h}{\partial\phi}(\tilde{u}^2-1)+\frac{1}{\mathrm{Re}}\frac{\partial^2\tilde{u}}{\partial\psi^2}, \tag{5}$$

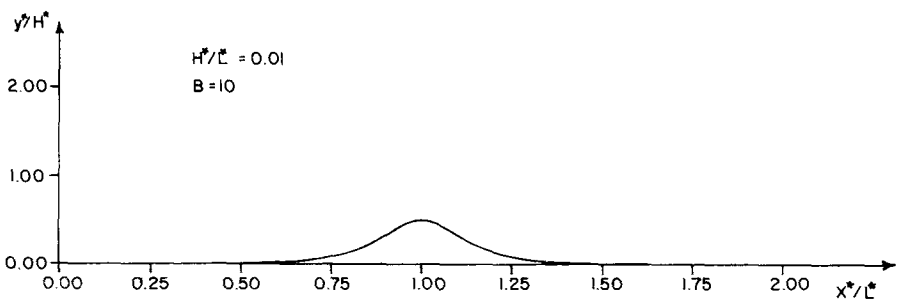


FIG. 1. Geometry of the curved wall.

$$\frac{\partial p}{\partial \psi} = 0, \tag{6}$$

$$\frac{\partial \tilde{u}}{\partial \phi} + \frac{\partial \tilde{v}}{\partial \psi} = 0. \tag{7}$$

The relation $h^2(\partial p/\partial \phi) = (1/h)(\partial h/\partial \phi)$, which is valid for the inviscid flow, has been used.

We introduce the Levy–Lees variables

$$\xi = \phi, \quad \eta = \psi(\mathrm{Re}/2\xi)^{1/2}, \tag{8}$$

$$F = \tilde{u}, \quad V = \tilde{v}(2\xi\,\mathrm{Re})^{1/2} - \eta F. \tag{9}$$

Then, the $\phi$ momentum and the continuity equations take the standard form

$$2\xi F F_\xi + V F_\eta + \beta_0(F^2 - 1) - F_{\eta\eta} = 0, \tag{10}$$

$$2\xi F_\xi + V_\eta + F = 0, \tag{11}$$

where the pressure gradient

$$\beta_0 = -\frac{2\xi}{h}\frac{\partial h}{\partial \phi} \tag{12}$$

is a function of $\phi$ and $\psi$. However, its deviation from the value at the surface (i.e., at $\psi = 0$) is $O(\mathrm{Re}^{-1/2})$, and hence, we evaluate it from

$$\beta_0 = -\frac{2\xi}{h(\phi, 0)}\frac{\partial h}{\partial \phi}\bigg|_{\psi=0}. \tag{13}$$

The boundary conditions for Eqs. (10) and (11) are

$$F = 0, \quad V = 0 \text{ at } \eta = 0, \tag{14}$$

and

$$F \to 1 \text{ as } \eta \to \infty. \tag{15}$$

The initial condition is

$$F = F(\xi_0, \eta) \text{ at } \xi = \xi_0. \tag{16}$$

In the present application, the initial profile is taken to be the Blasius profile and it is specified at $\xi = 0$. This is because the curved wall approaches a horizontal flat plate near its leading edge.

As an example, we consider a curved wall given by

$$y^* = H^* \operatorname{sech}[B(1 - x^*/L^*)], \quad \text{for } |x^*| < \infty, \tag{17}$$

where $H^*$ is the maximum height and $B$ is a constant. The variation in curvature of this wall is shown in Fig. 2 as a function of $x^*/L^*$. Equation (17) shows that $y^*$ decays exponentially as $x^* \to \pm\infty$. For moderate values of $B$ (about 10), $y^*/H^* \approx 2e^{-10}$ at $x^* = 0$, which is very small. Therefore, for the purpose of calculating the inviscid flow over the hump, we assume that the wall is specified by Eq. (17) in the interval $0 \leq x^*/L^* \leq 2$, and that it coincides with the $x^*$ axis outside this interval. The inviscid flow and, hence, $h$ and $\beta_0$ are calculated numerically using Davis' method.[29]

Once $\beta_0$ is determined from the inviscid flow solution, the solution of Eqs. (10) and (11) subject to the boundary and initial conditions, Eqs. (14)–(16), is obtained by using a finite-difference marching technique. A second-order accurate scheme is employed. A Newton–Raphson procedure is used to quasi-linearize the nonlinear terms in the momentum equation. Hence, the momentum and continuity equations are coupled in their linearized forms. This is known as the Davis coupled scheme (see Blottner[31]). The $\xi$ derivative is replaced by a three-point backward formula, whereas the $\eta$ derivatives are represented by central differences. At the first two streamwise locations, the profiles are taken to be the Blasius profile.

For the Falkner–Skan flows, $\beta_0$ is a constant and a self-similar solution for Eqs. (10) and (11) can be obtained. Since the equations are ordinary- rather than partial-differential equations, we use a fourth-order Runge–Kutta method coupled with a shooting technique to satisfy the two-point boundary conditions (14) and (15). The asymptotic condition (15) is satisfied at $\eta = 18$, which proved to be sufficiently large. The step size $\Delta\eta$ is taken to be 0.01 for all the numerical results presented in this paper.

For further reference, we define

$$U_0 \equiv hu = F, \tag{18a}$$

$$E_0 \equiv \frac{\sqrt{\phi}}{\sqrt{\mathrm{Re}}}\frac{\partial hu}{\partial \psi} = \frac{1}{\sqrt{2}}\frac{\partial F}{\partial \eta}, \tag{18b}$$

$$V_0 \equiv \sqrt{\mathrm{Re}\,\phi}\,hv = \frac{V + \eta F}{\sqrt{2}}, \tag{18c}$$

$$H_0 \equiv \phi\frac{\partial hv}{\partial \psi} = \frac{1}{\sqrt{2}}\frac{\partial V_0}{\partial \eta}, \tag{18d}$$

$$G_0 \equiv \sqrt{\mathrm{Re}}\,\phi^{3/2}\frac{\partial hv}{\partial \phi} = -\frac{1}{2}V_0 - \frac{\eta H_0}{\sqrt{2}} + \xi\frac{\partial V_0}{\partial \xi}. \tag{18e}$$

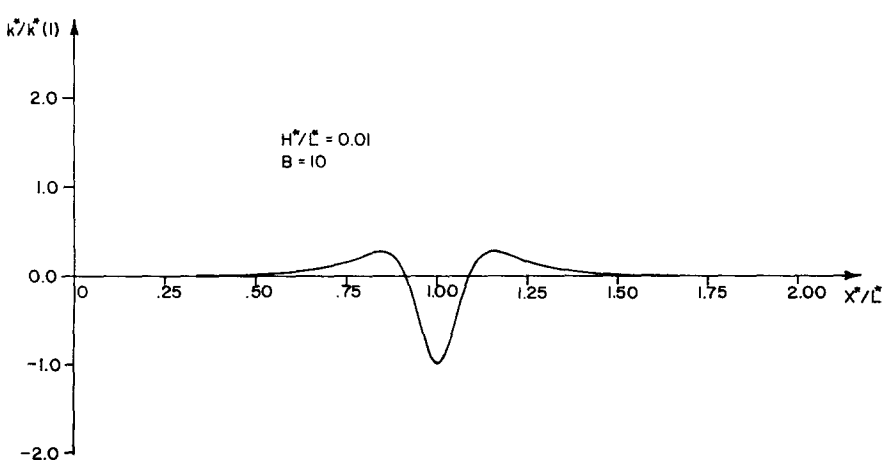


FIG. 2. Wall curvature distribution.

The behavior of the basic-flow solution as $\psi \to \infty$ is required. It follows from Eq. (15) that

$$U_0 \to 1, \quad E_0 \to 0. \tag{19}$$

Equation (11) can be rewritten as

$$\frac{\partial V}{\partial \eta} + 1 = (1 - F) + 2\xi \frac{\partial (1 - F)}{\partial \xi},$$

which upon integration with respect to $\eta$ yields

$$V + \eta = \int_0^\eta (1 - F) d\eta + 2\xi \frac{\partial}{\partial \xi} \int_0^\eta (1 - F) d\eta .$$

The integral in this equation is finite. As $\eta \to \infty$ it is proportional to the displacement thickness, hence

$$V + \eta \to \sqrt{2}\, g(\xi) \quad \text{as} \quad \eta \to \infty,$$

where $g(\xi)$ is a function of $\xi$. For the Falkner–Skan profiles, $g(\xi)$ becomes an absolute constant that depends on $\beta_0$. For the Blasius flow this constant is 0.8604. Therefore,

$$V_0 \to g(\xi) \quad \text{as} \quad \psi \to \infty, \tag{20a}$$

$$H_0 \to 0 \quad \text{as} \quad \psi \to \infty, \tag{20b}$$

$$G_0 \to -\frac{1}{2} g(\xi) + \xi \frac{dg}{d\xi}. \tag{20c}$$

It is worth noting that the transverse component of velocity $V_0$ and its streamwise derivative $G_0$ do not vanish outside the boundary layer. This is because the displacement thickness effect is neglected in the theory thus presented. However, we consider the flow due to the displacement thickness and its influence on the stability characteristics only for the Blasius flow. Also, we note that the transverse component of the boundary-layer solution in the present coordinate system does not grow indefinitely as $\psi \to \infty$ for a nonzero pressure gradient. This is in contrast with the behavior of the $v$ component in the body-oriented axes where it grows linearly with $y$ as $y \to \infty$. Therefore, we identify the present coordinate system as optimal to first order. Had we used the stream lines and potential lines of the inviscid flow over the displacement body we would have obtained optimal coordinates to second order.[32-34] In such coordinates the behavior of the boundary-layer solution produces the inviscid outer flow to second order (i.e., it includes corrections due to displacement thickness).

Van Dyke[32] showed that the outer solution of the stream function $\Psi^o$ for the second-order Blasius flow is

$$\Psi^o = y - \frac{\beta_1 \sqrt{2}}{\sqrt{\mathrm{Re}}} \mathrm{Re}(x + iy)^{1/2}, \tag{21}$$

and the inner solution is

$$\Psi^i \sim (2x/\mathrm{Re})^{1/2} f_1[y(\mathrm{Re}/2x)^{1/2}], \tag{22}$$

where $x$ and $y$ are Cartesian coordinates (they are identical to $\phi$ and $\psi$ for the case of a flat plate), $f_1(\eta)$ is the Blasius profile, and $\beta_1 = 1.21678$. A second-order composite expansion can be formed from $\Psi^o$ and $\Psi^i$ according to

$$\Psi^c = \Psi^i + \Psi^o - (\Psi^i)^o,$$

or

$$\Psi^c = (2x/\mathrm{Re})^{1/2}\{f_1 + \beta_1[1 - \mathrm{Re}[1 + i(y/x)]^{1/2}]\}. \tag{23}$$

Now, the $v$ components and its $x$ derivative defined by Eqs. (18c) and (18e) become

$$V_{02} = V_{01} - \frac{\beta_1}{\sqrt{2}} + \frac{\beta_1}{\sqrt{2}} \mathrm{Re}\left(1 + i\frac{y}{x}\right)^{-1/2}, \tag{24}$$

and

$$G_{02} = G_{01} + \frac{\beta_1}{2\sqrt{2}} - \frac{\beta_1}{2\sqrt{2}} \mathrm{Re}\left(1 + \frac{iy}{x}\right)^{-3/2}, \tag{25}$$

where $V_{02}$ and $G_{02}$ include displacement effects while $V_{01}$ and $G_{01}$ do not. We note that

$$V_{01} \to \beta_1/\sqrt{2}, \quad G_{01} \to -\beta_1/2\sqrt{2},$$

as $y \to \infty$, and hence $V_{02}$ and $G_{02}$ vanish as $y \to \infty$, as they should.

## III. THE DISTURBANCE EQUATIONS

We consider the stability of a basic flow over a two-dimensional curved wall with respect to three-dimensional disturbances in the form of alternating streamwise vortices, known as the Görtler vortices. Thus, each total flow quantity $q(\phi, \psi, z)$ is expressed in the form

$$q = q_0(\phi, \psi) + q_1(\phi, \psi, z), \tag{26}$$

where the subscript "0" denotes a basic-flow quantity whereas the subscript "1" denotes a perturbation quantity. Substituting these total flow quantities into the Navier–Stokes equations, subtracting the basic-flow quantities, and keeping linear terms in the perturbation quantities, we obtain the disturbance equations.[30]

### A. Scaled variables

For the stability analysis of boundary layers, the characteristic length should be based on a reference boundary-layer thickness. Hence, we introduce the scaled variables

$$\bar{\phi} = \phi, \quad \bar{\psi} = \psi/\delta_0, \quad \bar{z} = z/\delta_0, \tag{27}$$

where

$$\delta_0 = (\phi_0/\mathrm{Re})^{1/2} \tag{28}$$

is a reference boundary-layer thickness evaluated at the streamwise location denoted by $\phi_0$. Also, we define a Reynolds number based on $\delta_0$ as

$$R = \delta_0 \mathrm{Re}. \tag{29}$$

In the scaled variables, the disturbance equations without any approximation become:

$\phi$-momentum equation:

$$\delta_0^2 \frac{\partial^2 \bar{u}}{\partial \bar{\phi}^2} + \frac{\partial^2 \bar{u}}{\partial \bar{\psi}^2} + h^2 \frac{\partial^2 \bar{u}}{\partial \bar{z}^2} - m^{1/2} V_0 \frac{\partial \bar{u}}{\partial \bar{\psi}} - U_0 R \delta_0 \frac{\partial \bar{u}}{\partial \bar{\phi}} + \left(mH_0 - \frac{1}{2} m\beta_0 U_0 + m^{1/2} V_0 h K_\psi - \delta_0^2 \frac{\nabla^2 h}{h}\right)\bar{u} - \left(m^{1/2} E_0 + \frac{m^{3/2}}{R^2} \beta_0 V_0\right)\bar{v} + \frac{m}{R^2} \beta_0 \frac{\partial \bar{v}}{\partial \bar{\psi}} - \frac{2h}{R} \delta_0 K_\psi \frac{\partial \bar{v}}{\partial \bar{\phi}} - \frac{h}{R} \delta_0 \frac{\partial \bar{p}}{\partial \bar{\phi}} = 0; \tag{30}$$

$\psi$-momentum equation:

$$\delta_0^2\frac{\partial^2\bar{v}}{\partial\bar{\phi}^2}+\frac{\partial^2\bar{v}}{\partial\bar{\psi}^2}+h^2\frac{\partial^2\bar{v}}{\partial\bar{z}^2}-m^{1/2}V_0\frac{\partial\bar{v}}{\partial\bar{\psi}}-U_0R\frac{\partial\bar{v}}{\partial\bar{\psi}}+\left(-mH_0+\frac{1}{2}m\beta_0U_0\right.$$
$$\left.-m^{1/2}V_0hK_\psi-\delta_0^2\frac{\nabla^2h}{h}\right)\bar{v}-(m^{3/2}G_0+2U_0R^2hK_\psi)\bar{u}$$
$$-m^{3/2}\beta_0\frac{\partial\bar{u}}{\partial\bar{\psi}}+2hK_\psi R\delta_0\frac{\partial\bar{u}}{\partial\bar{\phi}}-h\frac{\partial\bar{p}}{\partial\psi}=0\,; \tag{31}$$

$z$-momentum equation:

$$\delta_0^2\frac{\partial^2\bar{w}}{\partial\bar{\phi}^2}+\frac{\partial^2\bar{w}}{\partial\bar{\psi}^2}+h^2\frac{\partial^2\bar{w}}{\partial\bar{z}^2}-m^{1/2}V_0\frac{\partial\bar{w}}{\partial\bar{\psi}}-U_0R\delta_0\frac{\partial\bar{w}}{\partial\bar{\phi}}-h^2\frac{\partial\bar{p}}{\partial\bar{z}}=0\,; \tag{32}$$

continuity equation:

$$R\delta_0\frac{\partial\bar{u}}{\partial\bar{\phi}}+\frac{\partial\bar{v}}{\partial\bar{\psi}}+h\frac{\partial\bar{w}}{\partial\bar{z}}-\frac{1}{2}\beta_0m\bar{u}-hK_\psi\bar{v}=0\,; \tag{33}$$

where

$$\bar{u}=u_1\,,\quad \bar{v}=Rv_1\,,\quad \bar{w}=Rw_1\,,\quad \bar{p}=R^2p_1\,, \tag{34}$$

$$m=\phi_0/\phi\,,\quad K_\psi=\delta_0k_\psi=-\frac{\delta_0}{h^2}\frac{\partial h}{\partial\psi}\,, \tag{35}$$

$$\beta_0=-\frac{2\phi}{h}\frac{\partial h}{\partial\phi}\,, \tag{36}$$

and $U_0$, $V_0$, $E_0$, $H_0$, and $G_0$ are functions related to the basic flow through Eqs. (18a)–(18e).

We identify $\beta_0$ with the pressure gradient parameter defined by Eq. (12) and $k_\psi$ as the curvature of the inviscid streamlines. The value of $k_\psi$ at $\psi=0$ is the curvature of the wall. In general, $k_\psi$ is a function of $\phi$ and $\psi$.

### B. A normal mode solution

Equations (30)–(33) constitute a system of homogeneous linear partial-differential equations with variable coefficients. They are of the elliptic type. The class of disturbances considered here is the Görtler vortices; that is, the disturbances are periodic in the $z$ direction. The dependence on $\bar{z}$ can be eliminated from the disturbance equations once the wavelength of the periodic disturbances is specified. The result is a system of partial-differential equations in $\bar{\phi}$ and $\bar{\psi}$ as independent variables. For high Reynolds numbers, the basic-flow quantities are slowly varying with $\bar{\phi}$. Consequently, the basic flow can be considered quasi-parallel, thereby allowing the separation of $\bar{\phi}$ from the disturbance equations. Hence, we evaluate the basic-flow variables at a fixed location, say $\phi_0$, follow Smith,[20] and assume the solution in the normal-mode form

$$\bar{u}_1=u(\bar{\psi})\cos\alpha\bar{z}\exp\left(\int\bar{\sigma}\,d\bar{\phi}\right), \tag{37a}$$

$$v_1=R^{-1}v(\bar{\psi})\cos\alpha\bar{z}\exp\left(\int\bar{\sigma}\,d\bar{\phi}\right), \tag{37b}$$

$$w_1=R_w^{-2}(\bar{\psi})\cos\alpha\bar{z}\exp\left(\int\bar{\sigma}\,d\bar{\phi}\right), \tag{37c}$$

$$p_1=R^{-2}p(\bar{\psi})\cos\alpha\bar{z}\exp\left(\int\bar{\sigma}\,d\bar{\phi}\right), \tag{37d}$$

where the spatial growth rate is denoted by $\bar{\sigma}$ instead of $\beta$, because $\beta_0$ is used to represent the pressure gradient. Substituting Eqs. (37a)–(37d) into Eqs. (30)–(33), we obtain

$\phi$-momentum equation:

$$u''-V_0u'+(H_0-h^2\alpha^2-\sigma U_0-\tfrac{1}{2}\beta_0U_0)u-E_0v+\Gamma_1=0\,; \tag{38}$$

$\psi$-momentum equation:

$$v''-V_0v'+(-H_0-h^2\alpha^2-\sigma U_0+\tfrac{1}{2}\beta_0U_0)v-(2U_0hG_N^2+G_0)u$$
$$-\beta_0u'-hp'+\Gamma_2=0\,; \tag{39}$$

$z$-momentum equation:

$$w''-V_0w'+(-h^2\alpha^2-\sigma U_0)w+h^2\alpha p+\Gamma_3=0\,; \tag{40}$$

continuity equation:

$$v'+(\sigma-\tfrac{1}{2}\beta_0)u+h\alpha w+\Gamma_4=0\,; \tag{41}$$

where

$$\sigma=\delta_0R\bar{\sigma}\,, \tag{42}$$

$$\Gamma_1=\left(V_0hK_\psi+\frac{\delta_0}{R}\frac{d\sigma}{d\bar{\phi}}+\frac{\sigma^2}{R^2}-\frac{\delta_0^2\nabla^2h}{h}\right)u-\frac{1}{R^2}(\beta_0V_0+2hK_\psi\sigma)v$$
$$+\frac{\beta_0}{R^2}v'-\frac{h\sigma}{R^2}p\,, \tag{43}$$

$$\Gamma_2=\left(-V_0hK_\psi+\frac{\delta_0}{R}\frac{d\sigma}{d\bar{\phi}}+\frac{\sigma^2}{R^2}-\delta_0^2\frac{\nabla^2h}{h}\right)v+2hK_\psi\sigma u\,, \tag{44}$$

$$\Gamma_3=\left(\frac{\delta_0}{R}\frac{d\sigma}{d\bar{\phi}}+\frac{\sigma^2}{R^2}\right)w\,, \tag{45}$$

$$\Gamma_4=-hK_\psi v\,, \tag{46}$$

$$G_N^2=R^2K_\psi\,, \tag{47}$$

and the prime denotes differentiation with respect to $\bar{\psi}$.

The variation of the streamline curvature in the $\psi$ direction (i.e., normal to the wall) is included in the function $K_\psi$. Hence, in general, $G_N^2$ is a function of $\bar{\psi}$. We identify the value of $G_N$ at $\bar{\psi}=0$ as the Görtler Number. Recalling the definitions of $R$ and $K_\psi$, Eqs. (29) and (35), we see that the present definition of Görtler number is based on the reference boundary-layer thickness $\delta_0$, whereas the original parameter identified by Görtler is based on the momentum thickness $\delta_m$. However, the two thicknesses are related (e.g., for the Blasius profile $\delta_m=0.664\ \delta_0$).

The boundary conditions are

$$u=v=w=0\ \text{ at }\ \bar{\psi}=0\,, \tag{48}$$

$$u,\ v,\ \text{and}\ w\to0\ \text{ as }\ \bar{\psi}\to\infty\,. \tag{49}$$

The homogeneous system defined by Eqs. (38)–(41), (48), and (49) is an eigenvalue problem. The characteristic equation of this eigenvalue problem can, in principle, be expressed in the form

$$F(\alpha,\sigma,R)=0\,, \tag{50}$$

where $\alpha$ is the wavenumber, $\sigma$ is the spatial growth (amplification) rate, and $R$ is a reference Reynolds number. Because of the dependence of the basic flow on the wall geometry and the explicit existence of the metric coefficient $h$ and its derivatives in Eqs. (38)–

(41), the surface given by Eq. (50) is configuration dependent. That is, in general, each geometry may have different characteristic surfaces in the space $\alpha$, $\sigma$, and $R$.

### C. An equivalent system of first-order equations

Equations (38)–(41) are reduced to a system of first-order differential equations by letting

$$z_1 = u\,,\quad z_2 = u'\,,\quad z_3 = v\,,\quad z_4 = w\,,\quad z_5 = w'\,,\quad z_6 = hp\,.$$

The result is

$$z' = Az\,, \tag{51}$$

where $z$ is the vector

$$z = (z_1, z_2, z_3, z_4, z_5, z_6)^T \tag{52}$$

and $A$ is a matrix that can be written as the sum of two matrices according to

$$A = A_0 + \Delta A. \tag{53}$$

Here,

$$A_0 = \begin{bmatrix} 0 & 1 & 0 & 0 & 0 & 0 \\ \alpha^2 + \sigma U_0 - H_0 + \frac{1}{2}\beta_0 U_0 & V_0 & E_0 & 0 & 0 & 0 \\ -\sigma + \frac{1}{2}\beta_0 & 0 & 0 & -\alpha & 0 & 0 \\ 0 & 0 & 0 & 0 & 1 & 0 \\ 0 & 0 & 0 & \alpha^2 + \sigma U_0 & V_0 & -\alpha \\ -\Lambda & -\sigma - \frac{1}{2}\beta_0 & -(\alpha^2 + \sigma U_0 + H_0 - \frac{1}{2}\beta_0 U_0) & \alpha V_0 & -\alpha & 0 \end{bmatrix},$$

and

$$\Lambda = 2U_0 G_N^2 - \sigma V_0 + G_0 + \tfrac{1}{2}\beta_0 V_0\,, \tag{54}$$

and the matrix $\Delta A$ is given in Appendix A. We note that the matrix $A_0$ contains all the terms of $O(1)$, whereas the matrix $\Delta A$ contains all the higher-order terms. The boundary conditions for the system (51) are

$$z_1 = z_3 = z_4 = 0 \quad \text{at} \quad \bar{\psi} = 0\,, \tag{55}$$

$$z_1,\ z_3,\ \text{and}\ z_4 \to 0 \quad \text{as} \quad \bar{\psi} \to \infty\,. \tag{56}$$

We recall the fact that the Görtler number $G_N$ in Eq. (54) is a function of $\bar{\psi}$.

The reduction of the governing equations to a system of six first-order equations requires the first derivatives of the basic-flow quantities. In the work of Smith,[20] Kahawita and Meroney,[26,27] and Floryan and Saric,[28] the disturbance equations were reduced to two coupled equations, one of second order in the $u$ component and the other of fourth order in the $v$ component. Then, the new equations were reduced to a system of six first-order equations, whose coefficients contain second-order derivatives of the basic flow, which demands a higher accuracy of the basic-flow solution than is required in the present method.

We define a basic system as

$$z' = A_0 z \tag{57}$$

subject to the boundary conditions (55) and (56). A method for solving the basic system is presented in Sec. IV. In Sec. V, a perturbation procedure is presented to obtain the correction to the eigenvalues due to a small deviation of the coefficient matrix $A$ from a basic value $A_0$.

## IV. A METHOD FOR SOLVING THE BASIC SYSTEM

The system (57) subject to boundary conditions (55) and (56) is a two-point boundary-value problem. Any one of the parameters $\alpha$, $\sigma$, and $R$ can be treated as the eigenvalue when the other two parameters are prescribed. An alternative to the parameter $R$ is the Görtler number $G_N(0)$ based on the wall curvature, in which case we rewrite Eq. (54) as

$$\Lambda = 2U_0 G_N^2(0) r(\bar{\psi}) - \sigma V_0 + G_0 + \tfrac{1}{2}\beta_0 V_0\,, \tag{58}$$

where $r(0) = 1$. If the deviation of the curvature of the streamlines from the value at the wall is neglected, then $r \equiv 1$ for all $\bar{\psi}$ and $G_N(0)$ is the eigenvalue. However, for the purpose of the present section, $r$ is assumed to be

$$\begin{aligned} &r = r(\bar{\psi}) \quad \text{for} \quad 0 \le \bar{\psi} \le \bar{\psi}_m\,, \\ &r = r(\bar{\psi}_m) \quad \text{for} \quad \bar{\psi} > \bar{\psi}_m\,. \end{aligned} \tag{59}$$

The difference between $r(\bar{\psi})$ and $r(\bar{\psi}_m)$ for $\bar{\psi} > \bar{\psi}_m$ will be accounted for by the perturbation technique presented in Sec. V.

### A. Boundary conditions at infinity

Application of the asymptotic boundary conditions (56) at a finite value of $\bar{\psi}$ may lead to inaccurate results. However, outside the boundary layer (i.e., $\bar{\psi} > 10$), the system of equations has constant coefficients because

$$U_0 \to 1\,,\quad H_0 \to 0\,,\quad V_0 \to \bar{V}_0\,,\quad E_0 \to 0\,,\quad G_0 \to \bar{G}_0 \quad \text{as} \quad \bar{\psi} \to \infty\,,$$

where $\bar{V}_0$ and $\bar{G}_0$ are constants. Let us denote the constant value of $A_0$ outside the boundary layer by $C$ so that Eq. (57) becomes

$$z' = Cz\,. \tag{60}$$

Let us denote the characteristic roots of $C$ by $\lambda_1, \lambda_2, \ldots, \lambda_6$ where the $\lambda_n$ are given by

$$\lambda^2 - \bar{V}_0\lambda - (\alpha^2 + \sigma + \tfrac{1}{2}\beta_0) = 0\,, \tag{61a}$$

$$\lambda^4 - \bar{V}_0\lambda^3 - (2\alpha^2 + \sigma)\lambda^2 + \alpha^2\bar{V}_0\lambda + \alpha^2(\alpha^2 + \sigma - \tfrac{1}{2}\beta_0) = 0\,. \tag{61b}$$

We consider the case in which three of the $\lambda_n$ are positive real numbers, whereas the other three are negative real numbers. Let $\lambda_1$, $\lambda_2$, and $\lambda_3$ be the positive roots.

When $\beta_0 = 0$, the characteristic roots of $C$ reduce to

$$\alpha, \lambda_2, \lambda_3, -\alpha, \lambda_5, \lambda_6, \tag{62}$$

where

$$\lambda_2 = \lambda_3 = \tfrac{1}{2}\{V_0 + [V_0^2 + 4(\alpha^2 + \sigma)]^{1/2}\}, \tag{63a}$$

and

$$\lambda_5 = \lambda_6 = -\tfrac{1}{2}\{-V_0 + [V_0^2 + 4(\alpha^2 + \sigma)]^{1/2}\}. \tag{63b}$$

For the special case $\sigma = \alpha V_0$, Eq. (63b) gives

$$\lambda_5 = \lambda_6 = -\alpha,$$

so that $-\alpha$ is a root of multiplicity 3. When $\sigma < -\frac{1}{4}(V_0^2 + 4\alpha^2)$, Eqs. (63) show that $\lambda_2$, $\lambda_3$, $\lambda_5$, and $\lambda_6$ are complex. In this case, the real parts of five of the $\lambda_n$ are positive and the boundary conditions (55) and (56) cannot be satisfied. Consequently, the present model is not applicable to this case and it needs to be modified.

Now, an analytic solution to the system (60) can easily be obtained in terms of elementary functions. Then, this solution serves as the boundary conditions for the system (57) at $\bar{\psi}_m$. The numerical method of solution requires casting these boundary conditions in the form

$$Tz = 0 \quad \text{at} \quad \bar{\psi} = \bar{\psi}_m, \tag{64}$$

where $T$ is a $3\times 6$ matrix of rank three. In the existing literature (e.g., Ref. 28), $T$ may be a function of $\bar{\psi}$ and it is found by inverting a $6\times 6$ fundamental matrix solution $\Phi$. In this paper, we develop a $T$ that is independent of $\bar{\psi}$ and that is found without inversion of $\Phi$. To accomplish this, we use the following system of equations that is adjoint to the system

$$(z^*)' = -A_0^T z^*, \tag{65}$$

and note[35] that, if $\Phi^*$ is a fundamental matrix solution of Eq. (65), then $(\Phi^{*T})^{-1}$ is a fundamental matrix solution of Eq. (57). At $\bar{\psi} = \bar{\psi}_m$, Eq. (65) reduces to

$$(z^*)' = -C^T z^* = C^* z^*. \tag{66}$$

Next, we reduce the matrix $C^* = -C^T$ to a Jordan canonical form by using the similarity transformation

$$J^* = P^{*-1} C^* P^*. \tag{67}$$

When $\beta_0 \neq 0$, the $\lambda_n$ are distinct and their corresponding eigenvectors are orthogonal. In this case, $J^*$ is a diagonal matrix and $P^*$ is a matrix whose columns are the eigenvectors of $C^*$. We arrange these columns so that the positive eigenvalues appear in the first three rows. When $\beta_0 = 0$, $P^*$ is defined in Appendix B, where the characteristic roots in $J^*$ are arranged so that the first three roots are the positive roots. Then, using the transformation

$$z^* = P^* \xi^*, \tag{68}$$

we rewrite Eq. (66) outside the boundary layer as

$$(\xi^*)' = J^* \xi^*. \tag{69}$$

Using Eq. (68) and the fact that if $\Phi^*$ is a fundamental matrix solution of (66) then $(\Phi^{*T})^{-1}$ is a fundamental matrix solution of (60), we conclude that $T$ consists of the last three rows of $P^{*T}$. Using similar arguments, we find that the adjoint boundary conditions outside the boundary layer are

$$T^* z^* = 0 \quad \text{at} \quad \bar{\psi} = \bar{\psi}_m, \tag{70}$$

where $T^*$ consists of the last three rows of $P$. Here, $P$ is a nonsingular $6\times 6$ matrix such that

$$J = P^{-1} C P \tag{71}$$

is a Jordan canonical form. When $\beta_0 = 0$, $P$ is defined in Appendix B. A detailed alternate derivation of these boundary conditions is contained in Ref. 30.

### B. Numerical procedure

Numerical integration of these two-point boundary-value problems are obtained by using a computer code (SUPORT) developed by Scott and Watts.[36] The method of integration uses superposition coupled with an orthonormalization procedure and a variable-step Runge–Kutta–Fehlberg scheme. We fix the values of any two of the parameter $\alpha$, $\sigma$, and $G_N$, and consider the third one as an eigenvalue. We make an initial guess for the eigenvalue. Starting at the position $\bar{\psi} = \bar{\psi}_m$, we carry out the integration toward the wall $\bar{\psi} = 0$. One of the boundary conditions at the wall will not be satisfied if the guessed eigenvalue is not the exact value. A Newton–Raphson iteration process is used to obtain a better approximation of the eigenvalue. The computer code is designed such that the boundary condition that has to be iterated on is the last specified one. Hence, for the basic system we iterate on the condition $z_4 = 0$ at the wall. The condition of convergence was taken as

$$|z_4(0)/\hat{z}_4| < 10^{-6},$$

where $\hat{z}_4$ is the maximum value of $z_4$ in the domain of numerical integration. For the adjoint problem the condition was taken as

$$|z_6^*(0)/\hat{z}_6^*| < 10^{-6}.$$

These conditions were used for all the calculations presented in this paper because, when a higher accuracy was used, the changes in the eigenvalues were of $O(10^{-6})$.

## V. A PERTURBATION PROCEDURE TO ACCOUNT FOR SMALL DEVIATIONS IN THE MATRIX $A_0$

The matrix $A$ in Eq. (53) is expressed as the sum of two matrices $A_0$ and $\Delta A$, where the elements of $\Delta A$ are small compared with those of $A_0$. In Sec. IV we presented a method of solution for the basic system whose matrix is $A_0$. Now, we present a perturbation approach to find the change in the eigenvalue due to a small change $A_1$ in $A_0$. However, we need not identify the change $A_1$ as the matrix $\Delta A$ in Eq. (53). The matrix $A_1$ represents a general, however, small change in $A_0$; $A_1$ may incorporate, in addition to $\Delta A$, changes in the basic-flow quantities due to displacement speed and/or viscous curvature effects. Since the perturbation in the eigenvalue due to each higher-order effect is small, interaction between these effects is negligible. Hence, one may study the influence of each higher-order term independent of the others. This will point out which second-order terms are the most stabilizing or desta-

bilizing. This is helpful in the aerodynamic design of surfaces with regions of concave curvature.

We consider the eigenvalue problem

$$z' = (A_0 + \epsilon A_1) z , \tag{72}$$

with the boundary conditions (55) and (56). We assume that $\epsilon \ll 1$. First, we solve the basic system

$$z_0' = A_0 z_0 , \tag{73}$$

with the same boundary conditions. Let $\lambda_0$ denote the eigenvalue of this system. We expand the solution of the system (72) in the form

$$z = z_0 + \epsilon \zeta \tag{74}$$

and the eigenvalue as

$$\lambda = \lambda_0 + \epsilon \lambda_1 . \tag{75}$$

Since $A_0$ depends on the eigenvalue $\lambda$, we use the Taylor-series expansion

$$A_0(\lambda_0 + \epsilon\lambda_1) = A_0(\lambda_0) + \frac{\partial A_0}{\partial \lambda}\bigg|_{\lambda_0} \epsilon\lambda_1 + \dots . \tag{76}$$

Substituting Eqs. (74)–(76) into Eq. (72) and neglecting terms of $O(\epsilon^2)$, we obtain

$$\zeta' - A_0 \zeta = \left(\lambda_1 \frac{\partial A_0}{\partial \lambda}\bigg|_{\lambda_0} + A_1\right) z_0 . \tag{77}$$

The boundary conditions (55) and (56) give

$$\zeta_1 = \zeta_3 = \zeta_4 = 0 \quad \text{at} \quad \bar{\psi} = 0 , \tag{78}$$

$$\zeta_1, \zeta_3, \zeta_4 \to 0 \quad \text{as} \quad \bar{\psi} \to \infty . \tag{79}$$

Since the homogeneous problem obtained from the system (77)–(79) has a nontrivial solution, namely $z_0$, then the nonhomogeneous problem has a solution only if a solvability condition is satisfied.[35,37] To obtain this condition, we multiply Eq. (77) by the transpose of the solution $z_0^{*T}$ of the adjoint homogeneous problem, integrate the result from $\bar{\psi} = 0$ to $\bar{\psi} \to \infty$, and obtain

$$\lambda_1 = -\int_0^\infty z_0^{*T} A_1 z_0 \, d\bar{\psi} \left( \int_0^\infty z_0^{*T} \frac{\partial A_0}{\partial \lambda}\bigg|_{\lambda_0} z_0 \, d\bar{\psi} \right)^{-1} . \tag{80}$$

Hence, the eigenvalue of the original system (72) becomes

$$\lambda = \lambda_0 - \int_0^\infty z_0^{*T} \epsilon A_1 z_0 \, d\bar{\psi} \left( \int_0^\infty z_0^{*T} \frac{\partial A_0}{\partial \lambda}\bigg|_{\lambda_0} z_0 \, d\bar{\psi} \right)^{-1} . \tag{81}$$

The integrals in Eq. (81) have to be evaluated numerically. In the interval $0 \le \bar{\psi} \le \bar{\psi}_m$, the values of $z_0$ and $z_0^*$ are known from the numerical solution of the basic problem and its adjoint. For $\bar{\psi} > \bar{\psi}_m$, the analytic solution outside the boundary layer is used. The eigenvalue $\lambda$ in Eq. (81) can be identified as $\alpha$, $\sigma$, or $R$ and its alternative $G_N^2(0)$. However, from the structure of the matrix $A_0$, it is advantageous to identify $\lambda$ with $G_N^2(0)$ since in this case all elements in the matrix $\partial A_0/\partial\lambda$ are zero except one element. Let $D_{ij}$ denote an element of $\partial A_0/\partial\lambda$; hence, $D_{ij} = 0$ for all $i$ and $j$ except

$$D_{61} = -2U_0 r , \tag{82}$$

where $r$ is defined by Eq. (59). Thus, Eq. (81) gives

$$\lambda = \lambda_0 + \int_0^\infty z_0^* \epsilon A_1 z_0 \, d\bar{\psi} \left( 2 \int_0^\infty r U_0 z_6^* z_1 \, d\bar{\psi} \right)^{-1} , \tag{83}$$

where $z_1$ is the first component of $z_0$ and $z_6^*$ is the sixth component of $z_0^*$. In Eq. (83), $\lambda$ and $\lambda_0$ stand for $G_N^2(0)$ with and without the correction due $\epsilon A_1$, respectively.

As a first application, we consider the correction due to restricting the function $r(\bar{\psi})$ to be a constant for $\bar{\psi} > \bar{\psi}_m$. Let $B_{ij}$ denote an element of $\epsilon A_1$, then $B_{ij} = 0$ for all $i$ and $j$ except

$$B_{61} = \begin{cases} 0 & \text{for } \bar{\psi} \le \bar{\psi}_m , \\ 2U_0\lambda_0[r(\bar{\psi}_m) - r(\bar{\psi})] & \text{for } \bar{\psi} > \bar{\psi}_m . \end{cases} \tag{84}$$

We note that $U_0 = 1$ for $\bar{\psi} > \bar{\psi}_m$. Equation (83) gives

$$\lambda/\lambda_0 = (I_1 + I_3)/(I_1 + I_2) , \tag{85}$$

where

$$I_1 = \int_0^{\bar{\psi}_m} r U_0 z_6^* z_1 \, d\bar{\psi} , \tag{86a}$$

$$I_2 = \int_{\bar{\psi}_m}^\infty r z_6^* z_1 \, d\bar{\psi} , \tag{86b}$$

$$I_3 = r(\bar{\psi}_m) \int_{\bar{\psi}_m}^\infty z_6^* z_1 \, d\bar{\psi} . \tag{86c}$$

As a second application of Eq. (83), we consider the effect of displacement thickness of the Blasius flow. It follows from Eqs. (24) and (25) that the perturbations in $V_0$ and $G_0$ are

$$V_1 = -\bar{V}_0[1 - \mathrm{Re}(t^{1/2})] , \tag{87}$$

$$G_1 = \tfrac{1}{2}\bar{V}_0[1 - \mathrm{Re}(t^{3/2})] , \tag{88}$$

where

$$t = [1 + i\bar{\psi}/\mathrm{Re}\,\phi_0)^{1/2}]^{-1} . \tag{89}$$

The nonzero elements of $\epsilon A_1$ are $B_{22} = V_1$, $B_{55} = V_1$, $B_{61} = \sigma V_1 - G_1$, and $B_{64} = \alpha V_1$. Then, Eq. (83) gives

$$\lambda = \lambda_0 + \int_0^\infty [V_1(z_2 z_2^* + z_5 z_5^* + \alpha z_4 z_6^* + \sigma z_1 z_6^*) - G_1 z_1 z_6^*] d\bar{\psi} \left( \int_0^\infty 2U_0 z_1 z_6^* \, d\bar{\psi} \right)^{-1} . \tag{90}$$

The destabilizing effect of $G_1$ is clear from Eq. (90) since its contribution to the integral is negative.

## VI. RESULTS AND DISCUSSION

Görtler[1] showed that the centrifugal instability of boundary-layer flows along concavely curved walls is primarily a function of the momentum thickness of the basic-flow profile and not of the details of the shape of the boundary layer. We recall that in Görtler's model the transverse component of the basic flow was neglected. This component was accounted for in the models of Smith[20] and Floryan and Saric.[28]

### A. The Blasius flow

Figure 3 shows the neutral stability curves for the Blasius flow obtained for different models. Curve 1 in Fig. 3 is Görtler's model. The pertinent equations are obtained from the basic system, Eq. (57), by setting $V_0 = G_0 = H_0 = 0$ for all $\bar{\psi}$ (i.e., we neglect the terms due to the transverse component of the basic flow). Curve 2 is the present model, curve 3 is the Floryan–Saric[28] mod-

el, and curve 4 is a modified Smith model. The governing equations of these three models are identical, Eq. (57). The differences among the neutral stability curves of these models, as shown in Fig. 3, are due to different treatments of the term $G_0$. In the present model, curve 2, $G_0 \to -\frac{1}{2}V_0 = -0.4302$ as $\bar{\psi} \to \infty$, as can be seen from Eq. (18e). Outside the boundary layer (i.e., $\bar{u} \approx 1.0$), the terms $V_0$ and $G_0$ represent the slope and curvature of the viscous streamlines, respectively. As discussed in Sec. II, these terms do not vanish outside the boundary layer in both the first- and second-order boundary-layer solutions. However, as $\eta \to \infty$ they vanish only in the second-order solution when we account for the displacement-thickness effect. Floryan and Saric,[28] in the calculation of curve 3, put $\partial V_0/\partial\phi_1 = 0$ for $\bar{\psi} \geq \bar{\psi}_m$, where $\phi_1 = \epsilon_v\phi$ and $\epsilon_v = 1/R$. We recall that in the Smith[20] model, the term $\partial hv/\partial\phi$ was not included in the analysis. Hence, in the modified Smith model, curve 4, we let $G_0 = 0$ for all $\bar{\psi}$.

We note that $\bar{\psi}_m = 12$ was used for all the calculations presented in Fig. 3. The accuracy of the solution was tested against changes in $\bar{\psi}_m$. Increasing $\bar{\psi}_m$ up to 24 produced insignificant changes, $O(10^{-6})$, in both the eigenvalues and the eigenfunctions. Also, the effect of the accuracy of the basic-flow solution was evaluated by using a second-order finite-difference scheme with $\Delta\eta = 0.01$ instead of the fourth-order Runge–Kutta scheme with $\Delta\eta = 0.01$. For the test case $\alpha = 0.01$, the change in the eigenvalue was insignificant $O(10^{-6})$, whereas the changes in the maximum values of the eigenfunctions were about 7%. This is consistent with the fact that the eigenvalue is a global value whereas the eigenfunction is a point solution. As a further test on the eigenvalues obtained for all the cases presented in this paper, the adjoint problem was solved and the obtained eigenvalues were compared with those of the basic system. The discrepancy between the two eigenvalues thus obtained was $O(10^{-5})$.

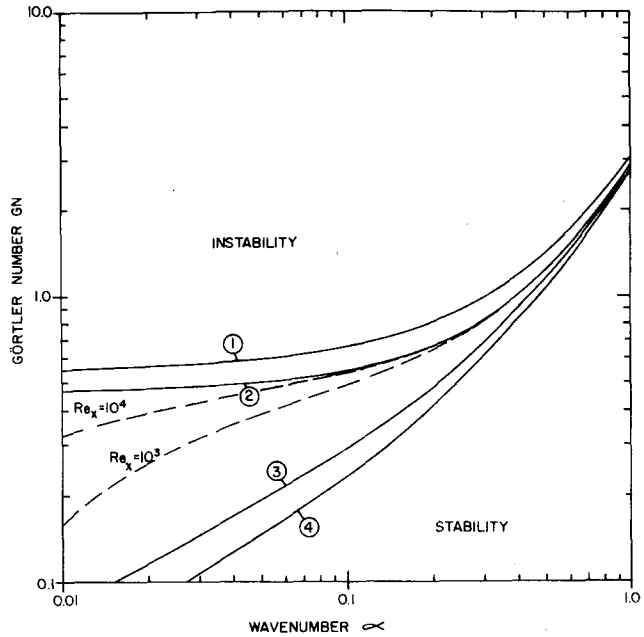


FIG. 4. Neutral stability of the Blasius flow; effect of displacement thickness. — Without displacement effect; --- with displacement effect.

### B. Effect of displacement thickness

The perturbation procedure presented in Sec. V was used to account for the effect of changes in the basic flow due to the displaced body on the neutral stability of the Blasius flow. Equations (87)–(89) show that the corrections $V_1$ and $G_1$ depend explicitly on the Reynolds number Re. We let $\mathrm{Re}_x$ denote $\mathrm{Re}\,\phi_0$. Figure 4 shows the neutral stability curves (the dashed lines) for the

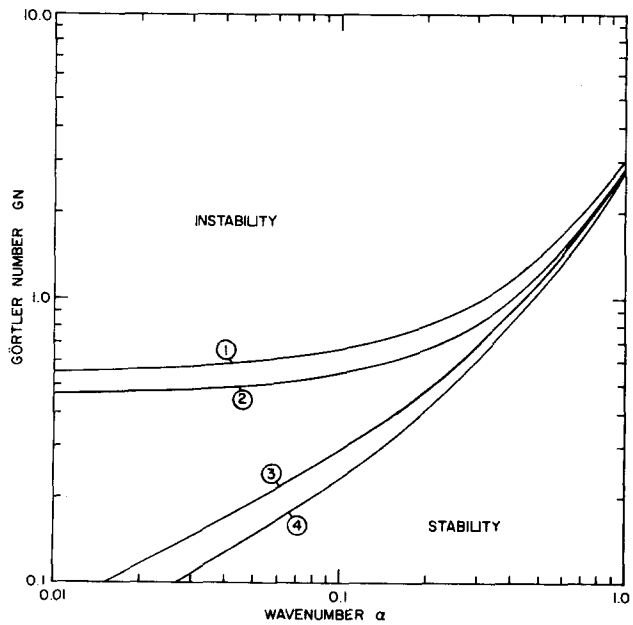


FIG. 3. Neutral stability for the Blasius flow; (1) the Görtler model, (2) the present model, (3) Floryan–Saric model, (4) the modified Smith model.

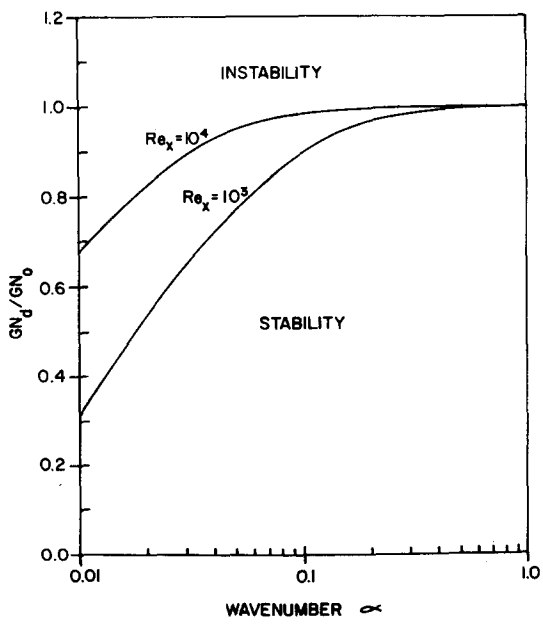


FIG. 5. Neutral stability of the Blasius flow; ratio of the Görtler number with displacement effect to the Görtler number without displacement effect.

Blasius flow with correction due to displacement speed for $Re_x = 10^3$ and $10^4$. It is clear from Fig. 4 that, for a given Reynolds number and wavenumber, the displacement-thickness effect is destabilizing for the Blasius flow. This effect is pronounced for small wavenumbers, which is expected because the disturbances extend farther outside the boundary layer, and there the changes in the basic flow due to the displaced body are important. Figure 5 shows the ratio of the Görtler number with displacement thickness effect accounted for to the Görtler number when this effect is absent. For a given Reynolds number, this ratio can be viewed as the ratio of the square root of the corresponding critical curvatures.

### C. Effect of decaying streamline curvature

Herbert[25] presented results for the Görtler model with streamline curvatures decaying exponentially away from the wall. Therefore, the function $r(\bar{\psi})$ in Eq. (59) has the form

$$r = \exp(-c\bar{\psi}), \tag{91}$$

where $c$ is a constant. In this case, an analytic solution for the system (60) can be obtained. However, in a more general situation, the variation of the streamline curvature is not exponential and it may be known only numerically. Since the perturbation procedure of Sec. V is not restricted to analytic representations of the streamline curvature, we used it to obtain the correction to the Görtler number due the variation specified by Eq. (91) as an example. For this case, the integral (86a) was evaluated numerically where the integral (86b) was obtained analytically. Figure 6 shows the neutral stability curve for $c = 0.1$. The Görtler number in this figure is based on the curvature of the wall (i.e., at $\bar{\psi} = 0$). Also shown in Fig. 6 is the calculation of Herbert using the Görtler model. We see that the decay of the streamline curvature stabilizes the flow. The stabilization effect is pronounced in the small wavenumber region. This is because for small wavenumbers the disturbances extend farther outside the boundary layer. As noted by Herbert,[25] the stabilizing effect of the decay in the streamline curvature from the value at the wall is due to the decrease in the driving centrifugal forces associated with the decreasing curvature.

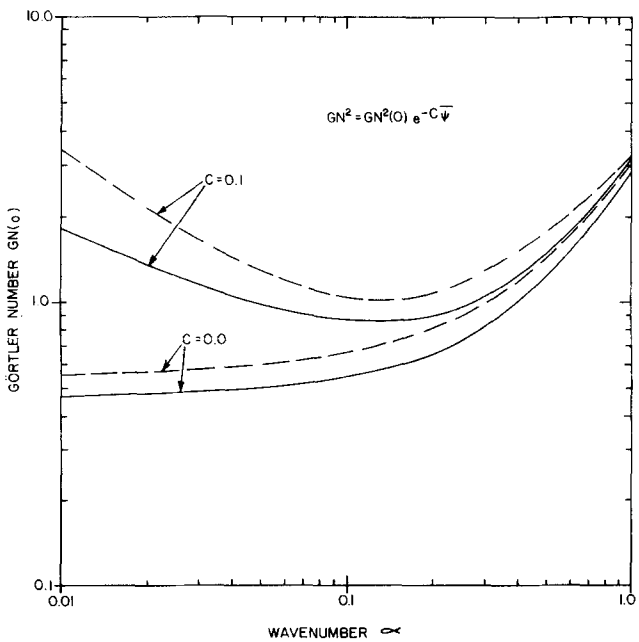


FIG. 6. Neutral stability of the Blasius flow; effect of decaying streamline curvature. --- Görtler model. —— present model.

### D. The Falkner-Skan profiles

The Falkner–Skan profiles correspond to constant values of the pressure-gradient parameter $\beta_0$ defined in Eq. (13). For flows along walls with general curvature variations, the boundary-layer solution is nonsimilar. The consideration of the self-similar solutions in this section is an approximation. That is, we patch the solution of the nonsimilar boundary layer to a self-similar profile that has the local value of the pressure-gradient parameter. This amounts to neglecting the history of the boundary layer up to the position under consideration and neglecting the gradient of $\beta_0$ at the local position.

Figure 7 shows the neutral stability curves for different values of the pressure-gradient parameter $\beta_0$. Favorable pressure gradients (i.e., $\beta_0 > 0$) are stabilizing. For $\beta_0 = 0.1$, the Görtler number shows a minimum at $\alpha \approx 0.09$. Adverse pressure gradients have a destabilizing effect. This effect diminishes as the wavenumber increases. All wavenumbers smaller than a certain value that depends on $\beta_0$ appear to be unstable. For $\beta_0 = -0.05$, the wavenumber at which there is no solution (i.e., no Görtler number) for neutral stability is $\alpha \approx 0.024$ and for $\beta_0 = -0.1$ it is $\alpha \approx 0.048$. We attribute this behavior to the normal component of the basic flow which increases as the pressure gradient becomes more adverse. By considering neutral stability,

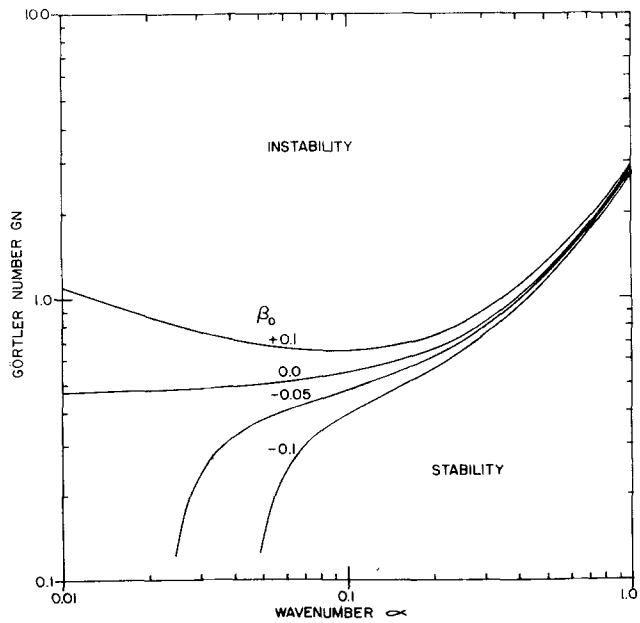


FIG. 7. Neutral stability for the Falkner–Skan flows.

we suppressed the change in the shape of the vortices in the downstream direction. This seems to be inconsistent with the growing boundary layer manifested by the transverse component $V_0$. By considering a parallel stream in the basic state (i.e., using the Görtler model for which $V_0 = H_0 = G_0 = 0$ for all $\bar{\psi}$) and for $\beta_0 = -0.1$, we obtained a curve on the $G_N - \alpha$ chart that is very similar to the case of no pressure gradient and there is no limiting wavenumber for neutral stability. The smallest wavenumber considered was $10^{-4}$. The value of $G_N$ asymptotically approaches 0.45 as $\alpha \to 0$.

Figure 8 shows the Görtler number for neutral stability as a function of $\beta_0$ in the range $-0.18 \leq \beta_0 \leq 0.1$ for $\alpha = 0.1$. The separation profile corresponds to $\beta_0 = -0.1988$. The stabilizing effect of favorable pressure gradients and the destabilizing effect of adverse pressure gradients are clear from this figure.

### E. Flows over a hump

We consider the curved wall given by Eq. (17). The inviscid flow solution was obtained using Davis' method. The nonsimilar boundary-layer equations, Eqs. (10)–(12), were solved by using a second-order accurate finite-difference scheme with $\Delta\eta = 0.01$ and $\Delta\xi = 0.005$. The asymptotic condition (15) was applied at $\eta = 8.4$, which corresponds to $\bar{\psi} = 11.8$. This value of $\bar{\psi}$ was taken as $\bar{\psi}_m$ for the stability computations.

The numerical values of the wall considered are

$$H^*/L^* = 0.01, \quad B = 10.0.$$

The maximum concave curvature is

$$k^*L^* = 0.2716 \quad \text{at} \quad x^*/L^* = 0.845.$$

The curvature is zero at $x^*/L^* = 0.915$. The maximum convex curvature is

$$k^*L^* = 1.0 \quad \text{at} \quad x^*/L^* = 1.0.$$

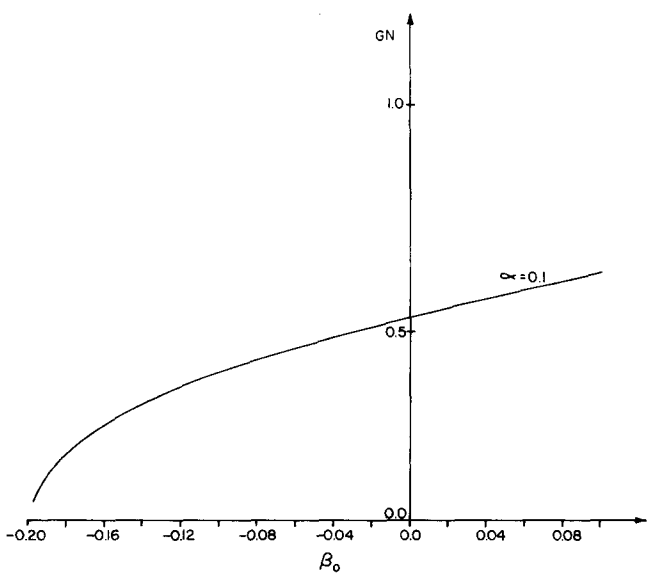


FIG. 8. Neutral stability for the Falkner–Skan profiles for wavenumber $\alpha = 0.1$.

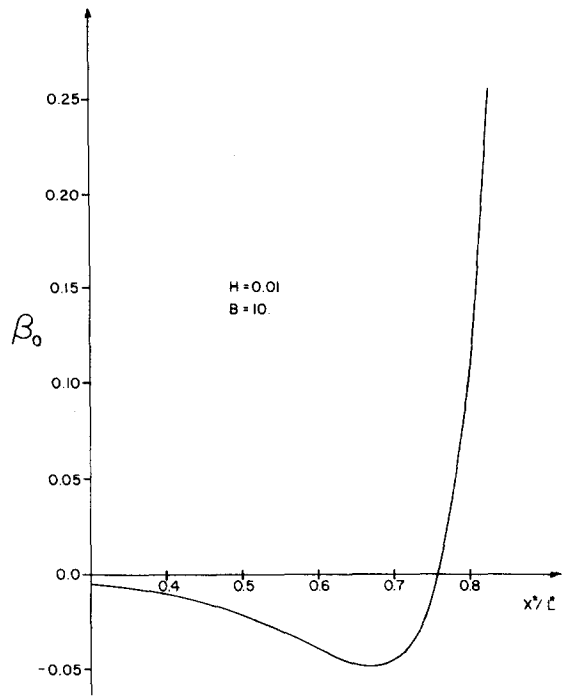


FIG. 9. Distribution of the pressure-gradient parameter $\beta_0$ for the hump.

The pressure-gradient parameter $\beta_0$ for this wall is shown in Fig. 9, whereas the curvature variation is shown in Fig. 2.

Figure 10 shows the growth rate $\sigma$ as a function of $x^*/L^*$ for vortices having the wavelength $\lambda^*/L^* = 0.166$

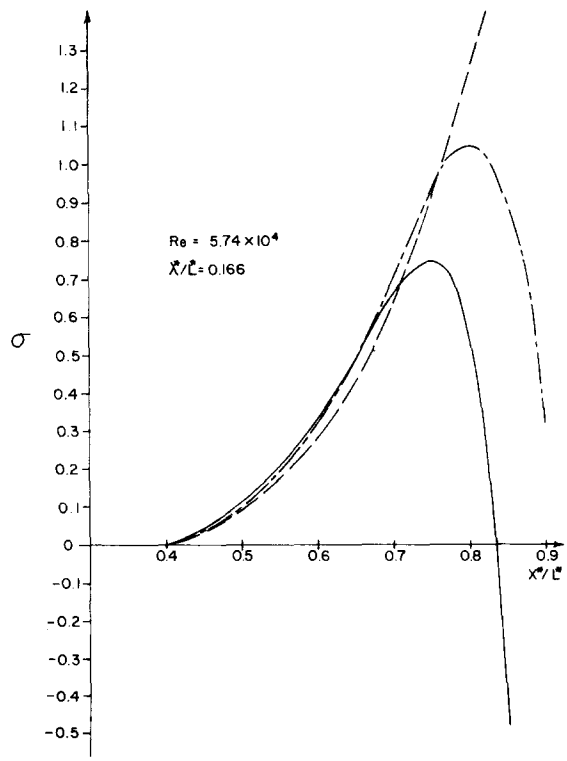


FIG. 10. Growth rates of Görtler vortices over a hump for the wavelength $\lambda^*/L^* = 0.166$. – – – Blasius profile. —— nonsimilar *B.L.* – – – – – local Falkner–Skan.

and $\mathrm{Re}=U_\infty^*\rho^*L^*/\mu^*=5.74\times10^4$. These values correspond to neutral stability at $x^*/L^*=0.4$. At this location $\beta_0=-0.011$ and $k^*L^*=0.00496$. We see from Fig. 10 that the vortices grow in strength in the downstream direction. The maximum growth rate appears at $x^*/L^*=0.75$. At this location $\beta_0=-0.01$ and $k^*L^*=0.154$. Downstream of $x^*/L^*=0.75$ the pressure gradient is favorable. The growth rate drops very rapidly to zero at $x^*/L^*\approx0.83$. At this location $\beta_0=0.283$ and $k^*L^*=0.2647$. Downstream of $x^*/L^*\approx0.83$, the vortices decay due to the favorable pressure gradient. Also shown in Fig. 10 are the growth rates of the same vortices calculated by using the Blasius profile and self-similar (Falkner–Skan) profiles. The agreement among these curves is reasonable in the region where the pressure gradient is slightly adverse. However, in the region of favorable pressure gradient, the Blasius and Falkner–Skan profiles overpredict by great amount the growth rates. Thus, using nonsimilar profiles is a must in determining the stability over such surfaces.

Since the submission of the present paper, Floryan and Saric[38] have corrected the results of Ref. 28.

## ACKNOWLEDGMENTS

This work was supported by the Fluid Dynamics Program of the Office of Naval Research and the Langley Research Center of the National Aeronautics and Space Administration under Grant NSG-1255.

## APPENDIX A: THE MATRIX $\Delta A$

The matrix $\Delta A$ is a $6\times6$ square matrix. The nonzero elements of this matrix are

$$a_{21}=(h^2-1)\alpha^2-V_0hK_\psi-\frac{\delta_0}{R}\frac{d\sigma}{d\bar\phi}-\frac{1}{R^2}\left(\sigma^2+\frac{1}{2}\beta_0^2-\beta_0\sigma-\phi_0\frac{\nabla^2h}{h}\right), \tag{A1}$$

$$a_{23}=(1/R^2)(\beta_0V_0+2\sigma hK_\psi-\beta_0hK_\psi), \tag{A2}$$

$$a_{24}=\beta_0h\alpha/R^2, \tag{A3}$$

$$a_{26}=\sigma/R^2, \tag{A4}$$

$$a_{33}=hK_\psi, \tag{A5}$$

$$a_{34}=-(h-1)\alpha, \tag{A6}$$

$$a_{54}=(h^2-1)\alpha^2-\frac{\delta_0}{R}\frac{d\sigma}{d\bar\phi}-\frac{\sigma^2}{R^2}, \tag{A7}$$

$$a_{56}=-(h-1)\alpha, \tag{A8}$$

$$a_{61}=\tfrac{1}{2}\beta_0hK_\psi+\sigma hK_\psi+\tfrac{1}{2}\beta_0'-2U_0(h-1)G_N^2, \tag{A9}$$

$$a_{63}=-(h^2-1)\alpha^2-2V_0hK_\psi+(hK_\psi)'+h^2K_\psi^2+\frac{\delta_0}{R}\frac{d\sigma}{d\bar\phi}+\frac{\sigma^2}{R^2}-\frac{\phi_0}{R^2}\frac{\nabla^2h}{h}, \tag{A10}$$

$$a_{64}=V_0(h-1)\alpha, \tag{A11}$$

$$a_{65}=-(h-1)\alpha, \tag{A12}$$

$$a_{66}=-hK_\psi. \tag{A13}$$

The prime denotes differentiation with respect to $\bar\psi$.

## APPENDIX B: THE MATRICES $P$ AND $P^*$

$$P=\begin{bmatrix}0&0&x_1&0&0&x_2\\0&0&\lambda_2x_1&0&0&\lambda_5x_2\\1&1&0&1&1&0\\-1&-\lambda_2/\alpha&-(\gamma+\sigma x_1)/\alpha&1&-\lambda_5/\alpha&-(\gamma+\sigma x_2)/\alpha\\-\alpha&-\lambda_2^2/\alpha&-\lambda_2(2\gamma+\sigma x_1)/\alpha&-\alpha&-\lambda_5^2/\alpha&-\lambda_5(2\gamma+\sigma x_2)/\alpha\\-(\overline{V}_0+\sigma/\alpha)&0&\gamma(2\alpha^2+2\sigma+\lambda_2\overline{V}_0)/\alpha^2&-(\overline{V}_0-\sigma/\alpha)&0&\gamma(2\alpha^2+2\sigma+\lambda_5\overline{V}_0)/\alpha^2\end{bmatrix}$$

where

$$\gamma=2G_N^2+\overline{G}_0,\quad x_1=-(\overline{V}_0/\alpha^2)[2\alpha^2+2\sigma+\lambda_2\overline{V}_0-\sigma(1-2\lambda_2/\overline{V}_0)],\quad x_2=-(\overline{V}_0/\alpha^2)[2\alpha^2+2\sigma+\lambda_5\overline{V}_0-\sigma(1-2\lambda_5/\overline{V}_0)],$$

$\lambda_2$ and $\lambda_5$ are defined by Eqs. (63a) and (63b), $\sigma\neq\alpha\overline{V}_0$.

$$P^*=\begin{bmatrix}\sigma x_2-(\overline{V}_0+\alpha)x_1&1&y_1&\sigma x_4-(\overline{V}_0-\alpha)x_3&1&y_2\\x_1&-\lambda_1^*/(\alpha^2+\sigma)&0&x_3&-\lambda_2^*/(\alpha^2+\sigma)&0\\(\alpha+\sigma/\alpha)x_2&0&(\alpha^2+\sigma)/\lambda_1^*&-(\alpha+\sigma/\alpha)x_4&0&(\alpha^2+\sigma)/\lambda_2^*\\-\overline{V}_0x_2&0&-\sigma/\alpha&\overline{V}_0x_4&0&-\sigma/\alpha\\x_2&0&\lambda_1^*/\alpha&-x_4&0&\lambda_2^*/\alpha\\x_2&0&1&x_4&0&1\end{bmatrix}$$

where

$$x_1=\gamma^*+\sigma^2/\alpha,\quad x_2=\sigma-\alpha\overline{V}_0,\quad x_3=\gamma^*-\sigma^2/\alpha,\quad x_4=\sigma+\alpha\overline{V}_0,\quad y_n=\sigma+\lambda_n^*[\gamma^*+\sigma(\alpha^2+\sigma)/\lambda_n^*-\sigma\lambda_n^*]/(\alpha^2+\sigma+\lambda_n^{*2}),\quad n=1,2,$$

and

$$\gamma^* = 2G_N^2 + \bar{G}_0 - \sigma\bar{V}_0\,, \quad \lambda_1^* = -\lambda_5\,, \quad \lambda_2^* = -\lambda_2\,,$$

$\lambda_2$ and $\lambda_5$ are defined by Eqs. (63a) and (63b),

$$\sigma \neq \alpha\bar{V}_0\,.$$


[1]H. Görtler, NACA Tech. Memo. 1375 (1954).
[2]M. Clauser and F. Clauser, NACA TN-613 (1937).
[3]H. W. Liepmann, NACA Wartime Report W-107 (1943).
[4]H. W. Liepmann, NACA Wartime Report W-87 (1945).
[5]N. Gregory and W. S. Walker, ARC Report M 2779 (1956).
[6]Y. Aihara, Bull. Aero. Res. Inst. Tokyo Univ. 3, 195 (1962).
[7]I. Tani and J. Sakagami, in *Proceedings International Council of Aerospace Science*, Stockholm, 1962 (Spartan, Washington, D.C., 1964), p. 391.
[8]F. X. Wortmann, in *Proceedings of the Eleventh International Congress of Applied Mechanics*, edited by H. Görtler (Springer–Verlag, Berlin, 1966), p. 815.
[9]F. X. Wortmann, AFOSR Report 64–1280, AF 61(052)-220 (1964).
[10]H. Bippes, NASA TM–75243 (1978).
[11]H. Bippes and H. Görtler, Acta Mechanica 14, 251 (1972).
[12]I. Tani, Adv. Aero. Sci. 3, 143 (1961).
[13]I. Tani, J. Geophys. Res. 67, 3075 (1962).
[14]I. Tani and Y. Aihara, Z. Angew. Math. Phys. 20, 609 (1969).
[15]F. X. Wortmann, J. Fluid Mech. 38, 473 (1969).
[16]Y. Aihara, Phys. Fluids 19, 1655 (1976).
[17]A. H. Nayfeh, J. Fluid Mech., 107, 441 (1981).
[18]G. Hämmerlin, J. Rat. Mech. Anal. 4, 279 (1955).
[19]G. Hämmerlin, Z. Angew. Math. Phys. 7, 156 (1956).
[20]A. M. O. Smith, Q. Appl. Math. 13, 233 (1955).
[21]F. Schultz–Grunow and D. Behbahani, Z. Angew, Math. Phys. 24, 449 (1973).
[22]D. Behbahani, Z. Angew. Math. Phys. 26, 493 (1975).
[23]G. Hämmerlin, Dtsch. Versuchsanst. Luft Raumfahrt, Ber. DVL-176 (1961).
[24]M. Tobak, Z. Angew. Math. Phys. 22, 190 (1971).
[25]T. Herbert, Arch. Mech. Stosow 28, 1039 (1976).
[26]R. A. Kahawitz and R. N. Meroney, Colorado State University, Fort Collins, Project Themis Technical Report No. 24 (1973).
[27]R. A. Kahawita and R. N. Meroney, J. Appl. Mech. 44, 11 (1977).
[28]J. M. Floryan and W. S. Saric, presented at the 12th AIAA Fluid and Plasma Dynamics Conference, Williamsburg, Virginia (1979), AIAA Paper No. 79–1497.
[29]R. T. Davis, presented at the 4th Computational Fluid Dynamics Conference, Williamsburg, Virginia (1979), AIAA Paper No. 79–1463.
[30]S. A. Ragab and A. H. Nayfeh, Virginia Polytechnic Institute and State University, Engineering Report No. VPI–E–79.41 (1979); also AIAA Paper 80-1377.
[31]F. G. Blottner, Comput. Meth. Appl. Mech. Eng. 6, 1 (1975).
[32]M. D. Van Dyke, *Perturbation Methods in Fluid Mechanics* (The Parabolic Press, Stanford, Calif., 1964), annotated edition 1975.
[33]S. Kaplun, Z. Angew. Math. Phys. 5, 111 (1954).
[34]R. T. Davis, University of Cincinnati, Department of Aerospace Engineering Report AFL 74–12–14 (1974).
[35]E. A. Coddington and N. Levinson, *Theory of Ordinary Differential Equations* (McGraw–Hill, New York, 1955), p. 70.
[36]R. R. Scott and H. A. Watts, SIAM J. Num. Anal. 14, 40 (1977).
[37]A. H. Nayfeh, *Introduction to Perturbation Techniques* (Wiley–Interscience, New York, 1981), Chap. 15.
[38]J. M. Floryan and W. S. Saric presented at the 13th Fluid and Plasma–Dynamics Conference of the American Institute of Aeronautics and Astronautics, Snowmass, Colorado, June 1980, Paper 80–1376.